TU Delft

Delft University of Technology

Document Version
Final published version

Licence
CC BY

Citation (APA)
Achilli, S., Marian, D., Lodari, M., Moreschini, L., Bonera, E., Scappucci, G., Pedrini, J., Virgilio, M., & Pezzoli, F. (2026). Optical spin pumping in silicon. *Physical Review Research*, *8*(2), Article 023302. https://doi.org/10.1103/cdkm-m3qc

Important note
To cite this publication, please use the final published version (if applicable).
Please check the document version above.

Copyright
In case the licence states “Dutch Copyright Act (Article 25fa)”, this publication was made available Green Open Access via the TU Delft Institutional Repository pursuant to Dutch Copyright Act (Article 25fa, the Taverne amendment). This provision does not affect copyright ownership.
Unless copyright is transferred by contract or statute, it remains with the copyright holder.

Sharing and reuse
Other than for strictly personal use, it is not permitted to download, forward or distribute the text or part of it, without the consent of the author(s) and/or copyright holder(s), unless the work is under an open content license such as Creative Commons.

Takedown policy
Please contact us and provide details if you believe this document breaches copyrights.
We will remove access to the work immediately and investigate your claim.

This work is downloaded from Delft University of Technology.

Optical spin pumping in silicon

Stefano Achilli,[1] Damiano Marian,[2] Mario Lodari,[3] Luca Moreschini,[3] Emiliano Bonera,[1] Giordano Scappucci,[3] Jacopo Pedrini,[1] Michele Virgilio,[2] and Fabio Pezzoli[1,*]

[1]*Dipartimento di Scienza dei Materiali, Università degli Studi di Milano-Bicocca and BiQuTe, Via Roberto Cozzi 55, 20125 Milano, Italy*

[2]*Dipartimento di Fisica, Università di Pisa, Largo Pontecorvo 3, I-56127 Pisa, Italy*

[3]*QuTech and Kavli Institute of Nanoscience, Delft University of Technology, 2600 GA Delft, Netherlands*

(Received 19 December 2025; accepted 9 May 2026; published 16 June 2026)

The optical generation of an out-of-equilibrium spin population is a keystone process for quantum technologies and spintronics alike. Although this is an established technique for studying direct band-gap semiconductors, it has been proven limited in materials that possess weak oscillator strengths for the optical transitions. We address the problem by presenting an all-optical analog of the spin-pumping method. By applying this concept to a Ge-on-Si heterostructure, we observe luminescence from Si with a polarization degree as high as 9%. The progressive etching of the absorbing layer, assisted by magneto-optic experiments, allows us to ascertain that the polarized emission is determined by effective spin injection aided by the carrier lifetime shortening due to extended defects. These findings can facilitate the use of highly promising spin-dependent phenomena of Si, whose optical exploitation has been hampered by fundamental limitations due to its peculiar electronic structure.

DOI: 10.1103/cdkm-m3qc

The ability to inject and detect spins in solid-state systems is of prime scientific and technological interest. Light-matter interaction in the presence of spin-orbit coupling has been shown to be one of the most effective strategies to achieve this purpose [1]. In semiconductors, the absorption of circularly polarized light transfers angular momentum to charge carriers, generating an out-of-equilibrium spin ensemble: a process commonly referred to as optical spin orientation [2,3]. The spontaneous evolution of the system toward thermal equilibrium can then occur through radiative recombination events. Due to the time reversal symmetry of the selection rules, spin-dependent optical transitions yield emission of circularly polarized light, making photoluminescence (PL) a convenient experimental tool for fast and contactless detection of the spin properties [2,3].

This all-optical injection-detection scheme was originally applied to direct gap semiconductors, such as GaSb [4] or GaAs [2], and lately contributed to gather a deeper understanding of the spin physics of emerging systems such as two-dimensional materials [5,6] and perovskites [7,8]. Despite all these advances, optical spin investigation continues to be highly ineffective for a large class of materials, namely, indirect gap semiconductors. The latter are jeopardized by the weak phonon-mediated transitions that make spin-dependent absorption and recombination inherently inefficient processes. The specific magnitude of the oscillator strength for these dipole-allowed transitions indeed results in (1) a weak spin-injection rate, washing out almost completely the average electron spin along the light propagation direction, and (2) a lengthening of the lifetime of the electrons in the fundamental indirect valleys to such an extent that spin relaxation occurs on a timescale faster than the recombination process, yielding, in other words, unpolarized PL.

The most prominent example in this context is Si, where experimental evidence for circularly polarized emission has long been awaited [9,10]. In this material, phonon-assisted transitions hinder resonant excitation at the indirect gap ($\sim$1.1 eV), while the complete spin relaxation also makes the excitation through the remote direct gap ($\sim$3.4 eV) impractical [11]. Various methods using highly polarizing magnetic fields [12,13], electro-optical hybrids [14,15], or purely electrical/thermal means [16–19] have been pursued as attempts to cope with the unfeasible, although more direct, measurement of the weak luminescence polarization. A recent work sets indeed the fundamental detection limit for the degree of polarization under convenient continuous-wave excitation to unpractical vanishing values of $\sim 10^{-4}$ [20], demonstrating that in Si the all-optical approach still remains a severe issue. Such a finding is in stark contrast with the fact that Si enabled the first experimental demonstration of optical spin injection in the solid state [1], and that the theoretical framework for such a process is now well understood [10,21,22].

In this work, we propose an alternative approach that circumvents the limitations of using optics to study indirect gap materials, and we illustrate it with Si as a prototypical semiconductor. Specifically, we mimic the technique of spin pumping [23,24] by introducing the optical analog depicted in the schematics of Fig. 1. Spin pumping relies on radio-frequency-induced magnetization dynamics to drive a spin current (J_S) across a semiconductor/ferromagnet interface

*Contact author: fabio.pezzoli@unimib.it

Published by the American Physical Society under the terms of the Creative Commons Attribution 4.0 International license. Further distribution of this work must maintain attribution to the author(s) and the published article's title, journal citation, and DOI.

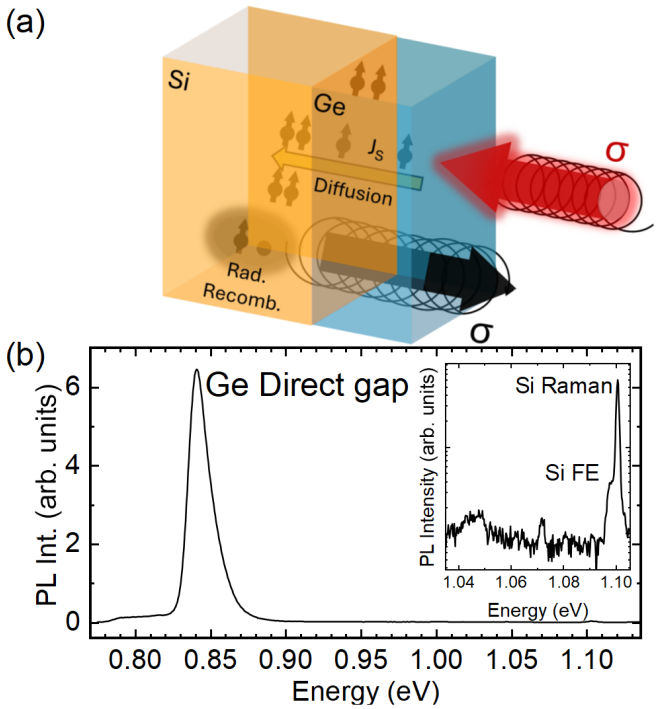


FIG. 1. Schematics of the optical spin-pumping effect. (a) Ge acts as a spin injector under optical excitation with circularly polarized light (σ, shown in red). Si functions as a spin sink and emits polarized luminescence (shown in black). The electron spin current J_S flows from Ge to Si because of diffusion gradient and thanks to the favorable band alignment. (b) Photoluminescence spectrum of the Ge/Si heterostructure measured at $T = 4$ K under excitation with a 1.165 eV laser, showing that the dominant peak is due to direct gap emission from the Ge epilayer. The inset shows a magnification at higher resolution in the spectral region of the Si band gap, highlighting from low to high energy: (1) low-intensity processes like the overtone Raman scattering or the recombination involving multiple emission of zone-center phonons and intervalley scattering (below ∼1.09 eV), (2) the free-exciton (FE) recombination involving transverse-optical (TO) phonons (at 1.097 eV), and (3) the one-phonon Raman mode (∼1.1 eV), respectively.

[25]. Here, instead, we apply optical orientation to excite a macroscopic magnetic moment and initiate spin dynamics in a light-absorbing medium. The latter replaces the ferromagnetic injector with a semiconducting film, which in our case is adjacent to Si and whose direct gap transitions must be suitably accessible. Inspired by a materials-by-design approach, our choice for the spin generator naturally falls on Ge. In addition to solving practical manufacturing constraints related to the epitaxy on Si and enabling integration in electronic and photonic devices, Ge offers highly polarized direct gap excitation [22,26–28] and a convenient band alignment at the interface with Si [29,30]. The band lineup spontaneously results in diffusion and transfer of spin-polarized electrons toward Si, even in the complete absence of an external electrical bias and without any impedance mismatch issue. This seemingly guarantees straightforward accumulation of a thermalized spin population directly in the Si sink, favoring radiative recombination events. Such profitable mechanisms, together with a shortening of the electron lifetime at the heterojunction, boast almost five orders of magnitude improvement of the circular polarization degree with an exceptional value as high as 9% [20]. The observation of the optical Hanle effect and a numerical model of the carrier photogeneration and diffusion process further corroborate such distinct result. The proposed approach can widen the access to intriguing spin-related properties of Si, whose optical exploitation has so far been narrowed due to the fundamental indirect nature of its electronic structure [31,32]. More generally, these findings have the potential to open innovative research directions in achieving spin injection and detection in spintronics and quantum technologies, harnessing materials that are technologically relevant and at the core of modern manufacture of electronic and photonic circuits.

I. MATERIALS AND METHODS

A. Sample structure

The Ge/Si heterostructure was grown on a Si wafer using a reduced-pressure chemical vapor deposition reactor. Starting with a 100 mm (001)Si substrate, a unintentionally doped 1.3 μm thick layer of Ge was grown using a dual-step process. An initial low-temperature (400 °C) growth of a Ge seed layer was followed by a higher-temperature (625 °C) overgrowth of a thick relaxed Ge buffer layer. Cyclic annealing at 800 °C was performed, yielding Ge under a residual tensile strain. For the Ge film, we estimated a p-type background doping of 2×10^{15} cm^{-3}, whereas the Si substrate is n type with a phosphorus donor concentration of 2×10^{15} cm^{-3}. We selectively etched the Ge film using a 0.1 M H_2O_2 solution with a 10 nm/min etching rate [33]. After each etching step, we monitored the thickness of the Ge film with a Veeco Dektak 8 profilometer.

B. Theoretical investigation

The electronic structure has been calculated by means of first neighbor tight-binding Hamiltonian, with $sp^3d^5s^*$ orbitals in both spin configurations. Strain has been included in the model to provide a more realistic description of the heterosystem, even though its relatively small value has negligible impact on the overall spin and charge dynamics. Since the presence of a type-II band discontinuity is accompanied by electrostatic effects due electron-hole charge displacement, the Hartree interaction potential has been taken into account in a self-consistent iterative scheme. A modified Scharfetter-Gummel discretization approach has been adopted to implement the Fermi-Dirac statistics [34,35]. Materials parameters are taken from the literature and are listed in the Supplemental Material [36]. We also included both direct and indirect optical absorption of the materials and the related pump depletion effects, and considered n- and p-type doping for Si and Ge, respectively. Pump reflection at the Si/Ge interface has been also implemented in the calculation.

C. Optical investigation and statistical analysis

PL measurements were carried out in a closed-circuit variable-temperature cryostat. The samples were excited by a circularly polarized Nd:YVO_4 laser at 1.165 eV. The power

density of the optical pump was on the order of kW/cm^2. The PL intensity was measured using a spectrometer equipped with an (In, Ga)As array detector. The polarization state of the PL was determined using a homemade polarimeter consisting of an optical retarder followed by a linear polarizer. Details about the determination of the polarization parameters associated with the PL polarization can be found in Refs. [28,37]. We computed the error bars of the polarization as standard deviations of different measurements to account for sample-to-sample variations related to possible unwanted control of the wet etching conditions. Statistical analysis and data presentation are based on the calculation of mean and standard deviations. Sample size for each statistical analysis is summarized in the Supplemental Material [36].

II. EXCESS CARRIER DYNAMICS IN GE/SI HETEROSTRUCTURE

Figure 1(b) shows a PL spectrum of a heterostructure composed of a Ge film epitaxially grown on a (001)Si wafer (see Sec. I for details). The measurement is carried out at a lattice temperature of 4 K using a Nd:YVO_4 laser at 1.165 eV to leverage the absorption through the direct gap of the epilayer. The spectrum is dominated by a peak at ∼0.84 eV, pertaining to the interband transitions in Ge occurring at the center of the Brillouin zone, i.e., the Ge direct gap [28,38]. Interestingly, in the energy range above the Ge band edge, at about ∼1.1 eV, an additional weaker signal can be resolved. A high-resolution measurement demonstrates the presence of various components. The most prominent one consists of a relatively brighter peak at 1.101 eV. Its energy separation from the laser line and its temperature-dependent behavior (see Sec. 1 of the Supplemental Material [36]) are consistent with the well-known one-phonon Raman spectrum of Si due to the zone-center longitudinal optical (LO) phonons. The surface-enhanced Raman scattering (SERS) origin can be ruled out since the observed feature matches the conventional first-order Si Raman mode and is measured in a planar epitaxial Ge/Si heterostructures rather than in a SERS-active interface. Yet, the magnified spectrum in Fig. 1(b) shows a set of minor bands observed at slightly lower energy, which are the superposition of second-order phonon Raman scattering [39,40] and low-intensity radiative recombinations [41].

Notably, the intense one-phonon Raman mode is superimposed to a weaker structure that appears as a redshifted shoulder at 1.097 eV. Such energy value is a strong indication that the likely source for this feeble component is the recombination of free excitons (FEs) that develop, also in this case, from the Si substrate [42,43]. Such FE emission is nevertheless spectrally resolved from the first-order Si Raman line in our high-resolution spectra, being separated by about 3 meV from the Raman peak, i.e., by more than three times the Raman full width at half maximum (∼1 meV). This ensures that the FE polarization can be analyzed independently of the Raman scattering contribution. Interestingly, the FE spectral line originates from a radiative recombination mediated by transverse-optical (TO) phonons, which is known to dominate the low-temperature PL spectrum of lightly doped unstrained Si [42,43]. The corresponding replica assisted by LO phonons is relatively weaker and blueshifted, hence potentially concealed by the one-phonon Raman peak. The formation of electron-hole droplets associated with the characteristic broad lower-energy emission has not been observed under our excitation conditions, pointing toward a low-injection regime [43]. The electronic nature of the FE peak is further confirmed by the observation of a Varshni-like temperature-induced behavior (see Sec. 1 of the Supplemental Material [36]). These experimental evidences strongly indicate that the PL emission from the buried Si substrate occurs alongside the direct photoexcitation of carriers in the overlying Ge film.

To explore the possibility of achieving spin-polarized optical recombination from Si, we begin by modeling the band structure around the Γ point of (001)Ge, considering a 0.2% biaxial strain caused by epitaxial growth at high temperatures [44–46]. The electronic spectrum shown in Fig. 2(a) has been calculated by means of first neighbor tight-binding Hamiltonian [47]. A tensile strain field is known to be induced upon cooling the Ge/Si heterostructure to cryogenic temperatures, due to the mismatch between the lattice thermal expansion coefficients of Si and Ge. This results in a splitting of the degeneracy of the light-hole (LH) and heavy-hole (HH) levels at the Γ point and in a reduction of the amplitude of the direct gap.

At the chosen pump energy, the vertical transition involving the split-off (SO) bands is active, as schematically depicted by the red arrow in Fig. 2(a). Those photoexcited electrons feature very small excess energy with respect to the conduction band edge, Γ_c. By virtue of the optical selection rules, a normally incident σ^+ circularly polarized excitation is expected to result for these SO-coupled electrons in a net spin polarization pointing along the quantization axis [Fig. 2(b)]. The latter is defined by the light propagation direction and corresponds with the growth direction, z. Due to energy conservation, electrons originating from the SO band, hence sitting close to the bottom of the Γ_c valley, are expected to provide a negligible contribution to the Si FE shown in Fig. 1(b). Rather, they primarily concur to the Ge recombination either through the directgap transitions or through L-valley indirect emission. The latter occurs upon intervalley scattering.

It is worth noting that the optical pump also excites conduction electrons from HH and LH bands [see arrows C and B in Fig. 2(a)]. As shown in Fig. 2(b), this electron population has the largest excess energy within the Γ_c ensemble and, at the same time, sustains a spin polarization (P_s) as high as ∼0.3. This value originates from the modest energy separation between the two valence bands and from the mixing of the total angular momentum J, induced by the finite value of the wave vector k. We therefore argue that such spin-polarized high-energy electrons can play a crucial role in the spin-pumping process.

To demonstrate that their intertwined spin and energy relaxation dynamics can eventually yield circularly polarized light also from the Si region, we show in Fig. 2(c) the valence (HH, LH, SO) and conduction (L, Γ_c, Δ) flat-band alignments between cubic Si and tensile-strained Ge, calculated following Refs. [48,49]. After photoexcitation in a neighbor of Γ_c of Ge, high-energy electrons can subsequently diffuse toward the heterojunction, while experiencing phonon-induced intervalley scattering toward the Δvalleys rather than the L valleys, owing to a larger transition rate [28]. Thanks to this process, these electrons can be eventually funneled into Si due to a

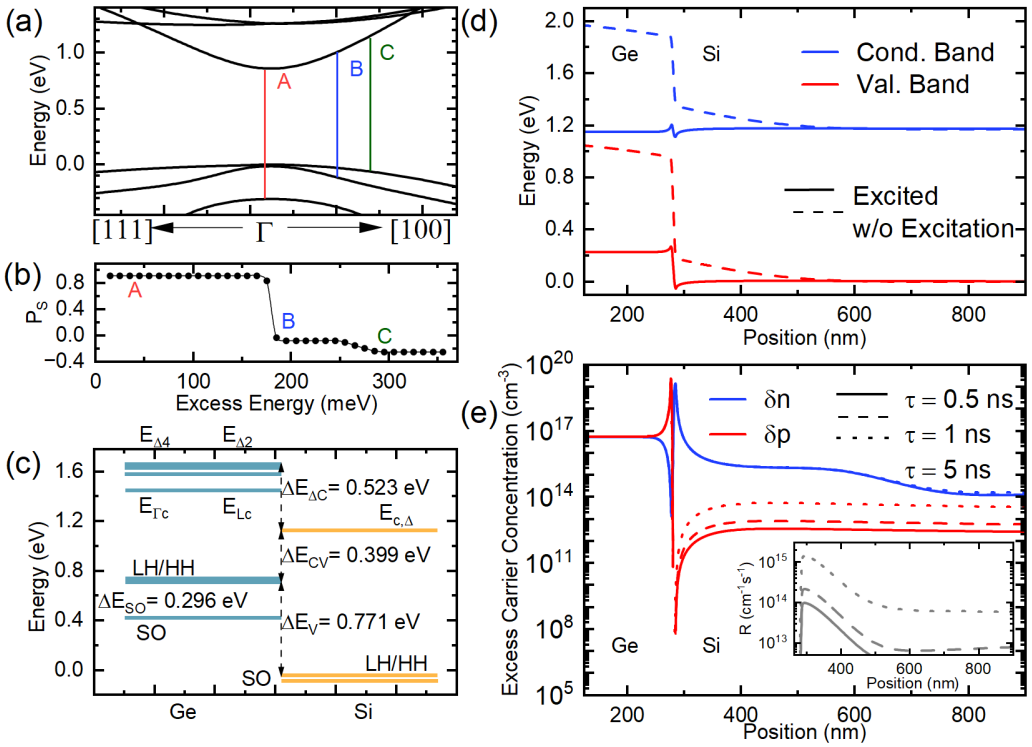


FIG. 2. Excess carrier modeling. (a) Low-temperature electronic spectrum of Ge under biaxial tensile strain of 0.2%. (b) Electronic spin polarization P_s as a function of the excess kinetic energy with respect to the bottom of the conduction band edge Γ_c. (c) Valence and conduction band edge alignments between cubic Si (yellow) and 0.2% strained Ge (light blue). (d) Valence (red) and conduction (blue) self-consistent band edge profiles for the *n*-type Si / *p* -type Ge heterojunction without (dashed) and with (solid) illumination (3 kW/cm^2) for $\tau_{Si} = 1$ ns. In panels (c) and (d), the reference energy is kept constant at the Si HH level. (e) Excess carrier concentration profiles δp (red) and δn (blue) in a neighbor of the heterointerface, calculated for different values of τ_{Si}. The inset reports the corresponding recombination rate R.

favorable band lineup (type II) with the Δ^{Si} band edge. In other words, an electron ensemble can be injected, virtually thermalized, at the absolute minimum of the Si conduction band. This can be particularly beneficial for enhancing the possibility of observing polarized PL, as it minimizes spin losses associated with energy relaxation and dwelling in the Si conduction band.

It should be also noticed that the robust potential barriers present at both the SO and HH/LH band edge profiles retain holes on the Ge side of the interface. It follows that the PL observed in Fig. 1(b) at the Si FE energy of 1.097 eV requires holes to be generated directly in the Si region. Direct photoexcitation in Si is indeed possible, although the resulting excess carrier concentration must be relatively small, since the absorption coefficient at the pump energy is modest, i.e., on the order of 10 cm^{-1}, and the type II band lineup tends to drain holes out of Si.

To quantitatively assess the excess carrier concentration profile, we have performed self-consistent drift-diffusion simulations considering the optically excited Si/Ge heterointerface in a two-band approximation, assuming that the large majority of electrons and holes populate the Δ valley and the HH band, respectively. Materials parameters are listed in Sec. 2 of the Supplemental Material [36] (see also Sec. I for further details) [34–36]. As for the recombination dynamics, we expect the excess carrier lifetime being dominated by a Shockley-Read-Hall mechanism, due to the well-known presence of lattice defects at the epitaxial interface [50–52]. Thus, we have modeled this recombination channel following Ref. [53] setting the same recombination time τ for electrons and holes. Due to the large uncertainty affecting the value of this materials parameter, which is strongly excitation and sample dependent, the simulations have been performed varying τ_{Si} in the Si region in the 0.5–5 ns range, while keeping a fixed value τ_{Ge} of 1 ns for the defective Ge layer [50].

In Fig. 2(d), we show the band edges at equilibrium (i.e., without illumination) for a typical sample with a Ge thickness of 280 nm. Using these parameters and the doping levels characterizing the two semiconductors forming the junction (see methods), the type II *p*-*n* heterojunction almost approaches a broken-gap condition, resulting in an energetic barrier for holes that is practically equal to the Si gap. Consequently, spin-polarized electrons experience a potential step roughly equal to the Ge gap.

When the sample is optically excited, with a pump fluency of, e.g., 3 kW/cm^2, a large density of carrier is created in the Ge region, resulting in a negative charge transfer to the Si material, triggered by the aforementioned potential step. Remarkably, the hole backflow, i.e., from Si to Ge, is much weaker because of the significantly smaller value of the absorption coefficient in Si with respect to Ge. As a result, a complete flattening of the conduction band edge profile and a lowering of the valence band discontinuity, whose value is now close to the gap difference between Si and Ge, can be observed.

The corresponding excess electron (hole) density $\delta n = n - n_{eq}$ ($\delta p = p - p_{eq}$) is reported in Fig. 2(e). Considering that bulk Si features a much larger excess carrier lifetime, this choice is motivated by the presence of crystal defects near the Ge interface acting as an efficient nonradiative recombination channel (see the following section discussing magneto-optical experiments). As expected, away from the Si/Ge junction the excess electron and hole concentration profiles flatten and tend to a common value (not shown in the figure for Si). Well inside the Si region, this quantity is controlled by the indirect absorption of the pump and varies in the 10^{12}–10^{13} cm^{-3} range, depending on the chosen τ_{Si}. Similarly, close to the top surface, the valence and conduction excess carriers have practically the same concentration, which for $\tau_{Ge} = 1$ ns is about 5×10^{16} cm^{-3}, due to the much larger optical absorption of Ge. Close to the interface, we observe an accumulation (depletion) of conduction carriers in the Si (Ge) region, with peak values exceeding 10^{18} cm^{-3}, triggered by the electron transfer from the Ge material and the attractive electrostatic interaction with holes confined in the epilayer. The same effect controls the sharp variation of hole concentration across the interface.

Using the carrier concentration profiles, we have estimated the spatially resolved radiative recombination rate $R = B(np - n_{eq}p_{eq})$, reported in the inset of Fig. 2(e), by varying τ. Here, B is the radiative recombination coefficient (see Sec. 2 of the Supplemental Material [36]). We find that R peaks at the interface, with values ranging from 10^{14} to 10^{15} s^{-1} cm^{-3}, decaying inside the Si material with a length scale of ∼100 nm. For comparison, we observe that similar R peak values in intrinsic bulk Si at low T require an excess carrier concentration $\delta p = \delta n \sim 10^{14}$–$10^{15}$ cm^{-3}. Finally, we have performed numerical experiments to consider also a spatial inhomogeneous crystal quality in Si, related to the quenching of the defects density far away from the Ge/Si interface. To this end, we have set larger excess carrier lifetimes for depths $\geqslant$400 nm. In this case, the main effect is the enhancement of the hole density close to the Si top surface, which is caused by the larger diffusion length of unpolarized holes generated deep inside the Si bulk. This results in a overall increase of the spatially resolved recombination rate, which, nevertheless, still peaks within 100 nm from the heterojunction.

In conclusion, the calculations indicate that the PL observed at the Si FE energy can be safely attributed to the optical recombination of electrons, originally excited in Ge by optical transitions from the HH/LH bands. These carriers efficiently diffuse in Si where they recombine radiatively with holes created therein by pump absorption through the indirect gap. Despite the small hole concentration in Si, the large electronic density due to carrier accumulation at the Si/Ge type II interface results in observable recombination rates R in the Si region in the proximity of the heterointerface.

This interesting mechanism leads to other notable conclusions. Electrons originating from HH/LH states can be remarkably polarized through optical orientation (see Fig. 2). The long-lived electron spins in Ge guarantee sizable spin diffusion along with reduced intervalley losses [54,55]. It is therefore reasonable to expect that optical spin pumping can take place in the heterostructure with Ge acting as an electron spin injector and Si serving as a spin sink. Even tough photogenerated holes will be almost unpolarized given their relatively short spin relaxation time, quite naturally radiative recombination events will involve the accumulated electron spins, potentially leading to the observation of a robust circularly polarized PL from Si. Therefore, once viewed in the framework of the type-II Ge/Si band lineup, the optical spin-pumping process is a direct consequence of the spontaneous transfer of spin-polarized electrons from Ge into Si, and the observation of circularly polarized Si FE emission can provide its experimental signature.

III. EXPERIMENTAL DEMONSTRATION OF THE OPTICAL SPIN-PUMPING EFFECT

To exploit the favorable band alignment and demonstrate the concept of optical spin pumping shown in Fig. 1(a), we performed optical spin orientation in Ge and analyzed the polarization pertaining to the Si FE emission. Specifically, the degree and state of polarization of the PL can be comprehensively characterized by measuring the modulation of the amplitude of the PL peak as a function of the relative orientation (analyzer angle) between an optical retarder and a polarizer [28,37,56].

This investigation was repeated while the Ge film was progressively thinned by selective wet etching until its full removal [33]. The outcomes, summarized in Fig. 3(a) under σ^+ excitation, unveil an intriguing scenario. The polarization analysis of the Si FE performed on the pristine Ge/Si heterostructure (i.e., Ge thickness 1.3 μm) shows indeed random fluctuations of the PL intensity, thus suggesting that only a minor fraction of the spin-oriented carriers is likely to be injected into Si. As a consequence, the polarized emission, if present, remains well below the noise level of the PL, akin to the conventional direct excitation of bulk Si. Such condition persists while further reducing the Ge thickness. Remarkably, as the thickness of the epitaxial layer approaches 0.55 μm, a net modulation of the PL starts to appear, revealing a sinusoidal behavior whose amplitude is enlarged by the subsequent etching steps. When the thickness of the Ge layer is reduced to 0.05 μm, the polarization curve clearly shows a distinct 90° periodicity oscillation with the largest peak-to-valley ratio. The latter is the hallmark of a significant circular polarization degree of the emission and is ultimately related to the optically oriented electron spins. This finding can also be better appreciated by having a close look at the corresponding PL spectra resolved in Fig. 3(b) for the σ^- and σ^+ polarizations. The former component is clearly larger than the latter both for the Raman mode and, most importantly, the Si FE (see Sec. 3 of the Supplemental Material for a derivation of the Raman selection rules under circular polarization [36]). Since the FE shoulder is spectrally resolved from the Raman peak in the high-resolution spectra, the larger intensity observed in Fig. 3(b) can be unambiguously assigned to the Si FE emission.

The transition from a featureless behavior to a full periodic modulation of the PL is also reflected in the degree of circular polarization, ρ. Figure 3(c) summarizes the statistical values retrieved from the polarization analysis conducted on several measurements on each sample. The precision in determining the epilayer thickness is intrinsically limited by the

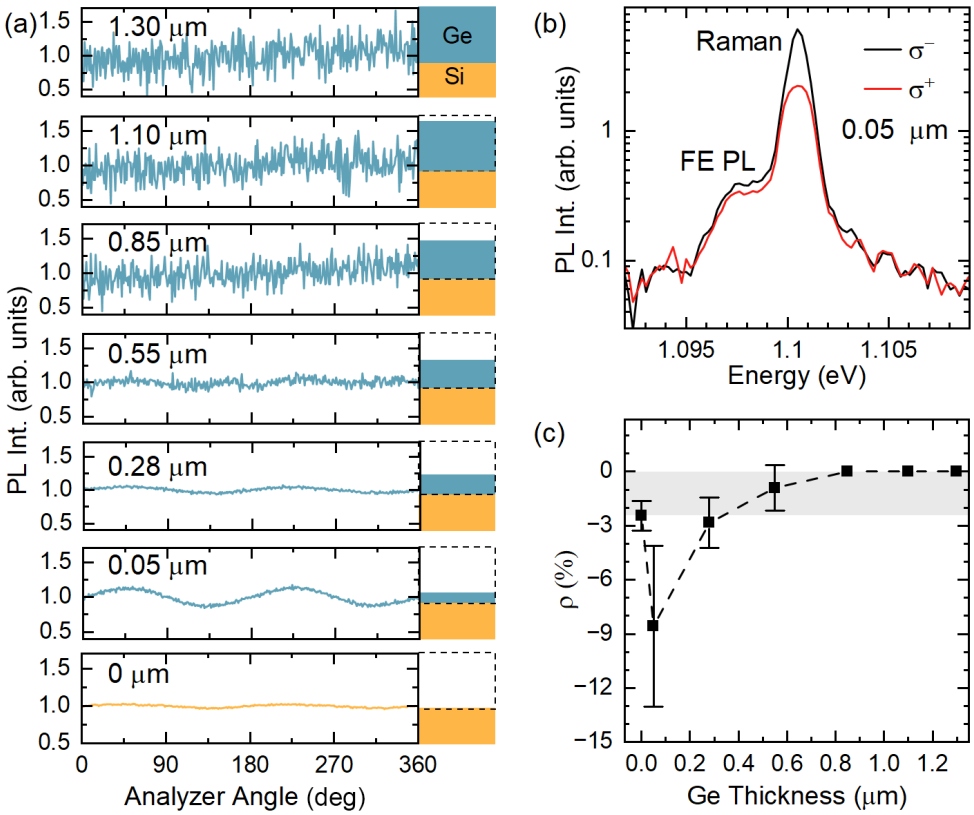


FIG. 3. Observation of polarized emission from Si. (a) Polarization analysis of the Si FE PL at 1.097 eV performed at $T = 4$ K as a function of the relative orientation (analyzer angle) between an optical retarder and a polarizer. The investigation is performed under σ^+ excitation for various Ge thicknesses by chemically etching the Ge film from 1.3 μm down to 0 μm. The latter corresponds to a complete removal of the Ge layer. (b) Polarization-resolved PL components of the Si FE measured at $T = 4$ K for a Ge thickness of 0.05 μm. The black curve corresponds to the left-handed, σ^-, component of the emitted light, whereas the red line shows the right-handed, σ^+, component. (c) Polarization degree ρ as a function of the Ge film thickness. The error bars are obtained from the standard deviation of several measurements, and the shaded region estimates the lower limit for the observation of spin-polarized emission.

reproducibility of the wet etching conditions, while the shaded area suggests a confidence region in which polarization is likely to be affected by signal-to-noise ratio limitations or systematic errors. Initially, when the Ge layer is thick, the PL is not polarized, so ρ is null. However, once the thickness of the Ge absorbing layer decreases, ρ becomes increasingly negative. These findings strongly support the emergence of circularly polarized PL from Si. Moreover, in striking agreement with the mechanism of optical spin pumping anticipated previously, the sign of the circular polarization of the Si FE demonstrates an opposite helicity with respect to that of the Ge direct gap (see Sec. 4 of the Supplemental Material [36]). Indeed, the latter originates from electrons optically coupled to the SO states. Their spin orientation is antiparallel to that of electrons photoexcited from the top of the valence band. These carrieres undergo intervalley scattering, which moves them out of the zone center and, after diffusion, produces the Si FE and its polarization. The PL helicity of Si is ultimately locked to that of Ge. The latter is itself nontrivially governed by the multivalley carrier and spin dynamics of Ge and has been extensively discussed and experimentally validated in previous work (Ref. [38] and references therein).

By further etching the sample, carriers are no longer generated in Ge, but rather in Si, and the Si polarization fades away as demonstrated in Fig. 3(c). Notice also the suppression of the amplitude oscillations in Fig. 3(a). Remarkably, ρ reaches a minimum when the Ge film is 0.05 μm thick with an absolute value $|\rho| = 9\%$ that is almost five orders of magnitude larger than what can be expected for resonant excitation at the steady state [20]. Therefore, we can argue that the previously described mechanisms of optical spin pumping and spin accumulation are indeed at play, outperforming conventional excitation schemes by providing a key strategy for injecting a giant spin polarization in Si and, more broadly, in indirect gap materials.

In the following, we will refine and expand our PL analysis to clarify this puzzling finding and test the role of optical spin pumping in determining the circular polarization of the Si FE. Figure 4(a) reports polarization-resolved spectra of the etched samples measured under σ^+, linear (Π), and σ^- excitation. Even though the largest polarization occurs at the energy of the Raman mode (∼50%), this effective polarization is clearly affected by a sizable polarized baseline that pertains to the broader FE PL. It can be noticed that the σ^- PL component dominates upon σ^+ excitation, while the opposite holds true when the helicity of the pump is reversed. This perfect mirrorlike behavior stems from the Kramers conjugation, making a compelling case for a spin-dependent radiative recombination. In addition, Fig. 4(a) consistently shows that when a Π pump is applied, the two σ-resolved spectra become

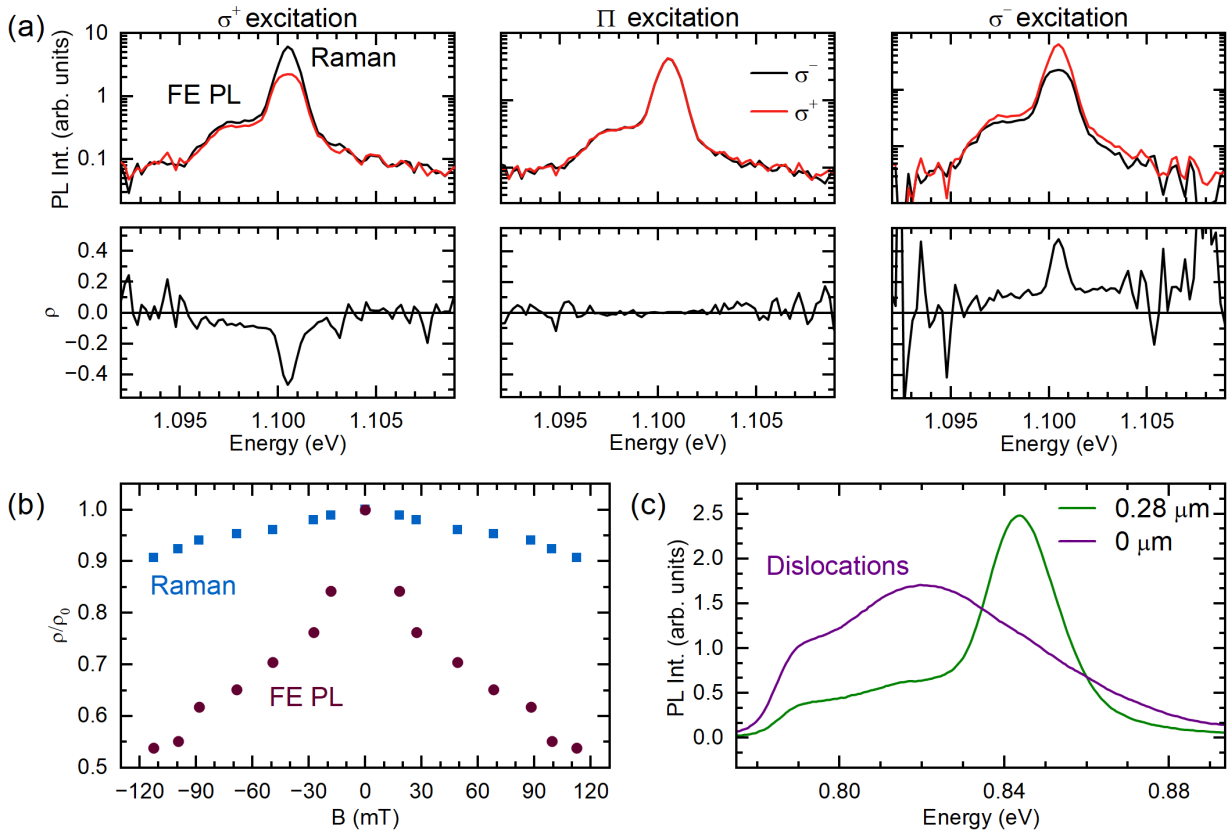


FIG. 4. Magneto-optical investigation. (a) PL spectra (top) and polarization degree ρ (bottom) measured by changing the helicity of the incident light. For each PL spectrum, the black (red) line corresponds to the σ^- (σ^+) component of the Si FE PL. (b) ρ as a function of a transverse magnetic field (Hanle effect) for the Raman line (blue squares) and for the Si FE PL (purple dots). The polarization is normalized to the zero-field value (ρ_0) and mirrored to negative fields to highlight the consistency with the expected Hanle line shape. (c) PL data in the spectral region of the direct gap of Ge for the samples with total Ge thickness equal to 0.28 μm (green) and 0 μm (violet). The spectral weight at low energy, peaked at 0.82 eV, is ascribed to dislocations in Si [57,58].

indistinguishable, in excellent agreement with the fact that no net out-of-equilibrium spin population can be expected under linear excitation. Further evidence of spin-related emission can be seen in the energy-resolved degree of the circular polarization [see Fig. 4(a)] since ρ switches sign for $\sigma^{\pm}$ and vanishes upon Π excitation. It is worth noting that the energy-resolved polarization associated with the Raman mode is characterized by a line that is evidently narrower than the spectral extension of the underlying ρ associated with the FE emission. Figure 4(a) therefore provides an additional demonstration that the sharp Raman contribution does not interfere with the polarization evaluated at the FE peak energy.

To provide conclusive proof of optical spin pumping in Si, we also conducted a dedicated magneto-optical investigation and leveraged the so-called Hanle effect [2,4]. This phenomenon is observed as a luminescence depolarization induced by a transverse magnetic field, i.e., orthogonal to the z axis, and originates from the decrease of the z projection of spin polarization because of the field-induced precession of the optically injected spins [20,59].

Figure 4(b) shows the field dependence of ρ for both the Raman and PL peaks pertaining to the Si substrate. The Raman mode undergoes only a moderate depolarization by increasing the magnetic field. Although we cannot rule out other spurious contributions, it seems reasonable that this apparent variation is affected by the behavior of the underlying broadened spectral component of the PL [see also Fig. 4(a)]. Indeed, the FE emission exhibits a drastic quenching, even in a weak magnetic field of just few milliteslas. This marked difference and the observation that luminescence exhibits a distinctive Hanle lineshape provide final compelling evidences of the spin-dependent nature of the polarized emission from Si.

Interestingly, the magneto-optical investigation discloses additional information, which is instrumental in understanding the spin dynamics characterizing the Ge/Si heterostructure. The full width at half maximum (ΔB) of the FE Hanle curve is given by [4,59]

$$\Delta B = 2\frac{\hbar}{g\mu_B T_S}, \tag{1}$$

where $\hbar$ the reduced Plank constant, μ_B the Bohr magneton, and g the electron Landé factor. T_S is the spin lifetime, which depends on the spin relaxation time τ_s and the carrier lifetime τ as

$$\frac{1}{T_S} = \frac{1}{\tau_s} + \frac{1}{\tau}. \tag{2}$$

Owing to the non-negligible circular polarization degree of the FE, it can be reasonably assumed that $\tau_s \gg \tau$, i.e., carriers recombine before completely losing their spin orientation. As

a consequence, $T_S \sim \tau$. Equation (1) can be used, knowing the well-established value of the electron g factor of Si, to estimate $\tau \sim 200$ ps. Such a characteristic time is extraordinarily short for an indirect band-gap transition: it is several orders of magnitude shorter than the typical minority lifetime, which in lightly doped Si wafers is in the ∼μs regime [60–62].

Such reduced lifetime ensures that in Si-based heterostructures carriers recombine while they are still spin polarized. This might also explain the observation of polarized FE emission when the Ge epilayer is fully removed by the wet chemical etching [Fig. 3(c)]. On the contrary, spin loss in a pristine Si wafer is known to occur on a timescale that is drastically faster than the carrier lifetime, thus precluding optical spin orientation to be identified through luminescence. We can find reassurance of such process by the complete absence of magnetic field dependence in control Hanle experiments conducted on a pristine Si wafer (see Sec. 5 of the Supplemental Material [36]).

A ultrafast lifetime is unexpected and hints at the presence of extrinsic mechanisms that in the Ge/Si heterostructures significantly accelerate the carrier dynamics compared to pristine bulk Si and might ultimately contribute to the spin-pumping process. Following the calculated carrier concentration profiles that show in Si a spatially resolved recombination rate peaked within 100 nm from interface, it is reasonable to expect that the drastic shortening of the lifetime is caused by the emergence of parasitic nonradiative channels in the proximity of the heterointerface. Crystal flaws, in the form of dislocations, are known to develop in the heteroepitaxial film because of the lattice mismatch with the substrate and are thus a likely culprit for the unexpected carrier kinetics. Such extended defects possess a large recombination velocity that can efficiently drain the photogenerated carriers, reducing the interband transition rate and shortening the excess carrier lifetime [59]. Although the defective interface does not preclude the use of Ge/Si in technological applications, it has been widely studied due to its impact on the radiative recombination in Ge [50–52,63]. Yet, no attention has been paid to its possible repercussions also on Si, and dedicated investigations are still awaited.

Figure 4(c) demonstrates that, in the low-energy range, the PL of the 0.28 μm thick Ge film (green, solid line) is dominated by the peak at about 0.84 eV due to recombination through the Ge direct gap [47]. Interestingly, this well-resolved PL appears to be superimposed onto a weaker but broader structure. This broad emission becomes evident in Fig. 4(c), observed when the Ge layer is completely removed by etching and the corresponding direct gap PL is suppressed. This previously hidden low-energy emission lies well below the Si band edge and indicates the presence of defect-induced energy levels within the Si band gap. The energy of this emission is indeed in excellent agreement with the well-established dislocation-related luminescence, the so-called D1 line [57,58]. The distinct presence of a D line in the low-energy PL spectrum of Si demonstrates that extended defects are injected into the substrate as also found in previous structural investigations [64]. Finally, it should be noted that defects developed at the Ge/Si interface might also provide an additional source of spin-flip scattering during the Ge-to-Si transfer. The luminescence polarization observed in Si should be thus regarded as the residual polarization that survives the competition between interfacial depolarization, if any, and the ultrafast carrier dynamics inferred from the Hanle analysis.

IV. DISCUSSION AND CONCLUSIONS

The direct experimental observation of circularly polarized emission in Si has been often considered difficult in the conventional framework of optical spin orientation, due to the negligible spin-injection rate and the extremely long carrier lifetime associated with indirect gap transitions. The measurable circular polarization accounts for the dynamical evolution of the spin ensemble given by carrier recombination and intrinsic spin relaxation. These processes effectively reduce the maximum spin polarization attainable at the moment of photoexcitation, $\rho_{\max}$, so that the degree of the PL at the steady state is $\rho = \frac{\rho_{\max}}{(1+\tau/\tau_S)}$. A sizable measurement of the polarization can thus be obtained whenever extrinsic means enable a strong suppression of τ compared τ_S, irrespective of the initial $\rho_{\max}$ value. Viable strategies to achieve this purpose include high optical excitation to enhance nonradiative Auger recombination, as very recently shown by Ref. [20]. The magneto-optical results further corroborated the optical spin-pumping approach in Si-based heterostructures.

Notably, this work demonstrates how to further increase the polarization of the Si PL by manipulating $\rho_{\max}$, hence overcoming the strict limitations hampering the direct optical excitation of unstrained Si. Under optical spin pumping at the steady state, a giant spin accumulation in Si can arise from the large diffusive current given by the electron spins originally photogenerated in Ge. As suggested by the diffusion model developed here, electrons optically coupled to the top of the Ge valence band can transfer spin angular momentum into Si up to an impressive maximum value of $|P_S| \simeq 30\%$ [see Figs. 2(a) and 2(b)]. Such spin-oriented carriers can then decay radiatively, thereby emitting circularly polarized PL.

Symmetry arguments applied to the optical selection rules of phonon-mediated transitions in Si predict an efficiency for the emission of circular polarization in unstrained Si of $\eta_{\mathrm{LO}} = 27.7\%$ and $\eta_{\mathrm{TO}} = 18.8\%$ for recombination involving LO and TO phonons, respectively. The LO/TO replicas should be cross-polarized [21,22]. Consequently, in complete absence of spin relaxation mechanisms, the maximum circular polarization degree of the $\mathrm{FE_{TO}}$ is expected to be $|\rho_{\max}| = \eta_{\mathrm{TO}} \times P_S = 0.188 \times 0.3 \sim 6\%$ when the TO/LO splitting can be resolved. Interference between the two optical phonons otherwise decreases the efficiency, which weighted for the relative luminescence intensity of the TO, I_{TO}, and LO, I_{LO}, phonons becomes $\eta_{\mathrm{eff}} = \frac{\eta_{\mathrm{TO}} I_{\mathrm{TO}} + \eta_{\mathrm{LO}} I_{\mathrm{LO}}}{I_{\mathrm{TO}} + I_{\mathrm{LO}}} = 13.3\%$ [13], thus yielding $|\rho_{\max}| = \eta_{\mathrm{eff}} \times P_S = 0.133 \times 0.3 \sim 4\%$. As a further reassurance of the effectiveness of the optical spin-pumping approach introduced here, we can notice that these expected values of $\rho_{\max}$ fall satisfactorily within the experimental uncertainty of the largest ρ reported in Fig. 3(c) for a Ge thickness of 0.05 μm. Since under this condition $\rho \simeq \rho_{\max}$, we can suggest that the injection in Si of electrons that are practically thermalized is a condition that is genuinely satisfied by the proposed optical spin-pumping approach and guaranteed by the band alignment established between the spin sink, i.e., Si, and the light-absorbing medium acting as

spin injector, i.e., Ge. This requirement is further aided by the ultrafast dynamics established by the extended defects. Essentially, the polarization of the spin current funneled into Si maps directly into the PL, giving rise to a nonmonotonic behavior in which an increase of ρ is initially observed in Fig. 3(c) compared to the case of pristine Si at low Ge coverage, and eventually the polarization shows an asymptotic tendency to unpolarized FE emision as the Ge epilayer approaches the micrometer range. Finally, we notice that the physical phenomena described in this work are not limited to Si, but can, in principle, be applied to every semiconductor architectures involving indirect gap materials with suitable band alignments. Moreover, optical spin pumping allows one to devise novel methods to increase the polarized emission. In Si, for instance, it can be expected that the use of an injector comprising low-dimensional Ge structures, such as quantum wells, can enlarge $\rho_{\max}$ to almost unitary values thanks to confinement-induced removal of the HH/LH degeneracy. This can be used in addition to other means such as applying strain, which has been presented by theoretical works as a strategy to (1) modify η by lifting the degeneracy of the valence band directly in Si [22] and (2) lengthen τ_S by suppressing intervalley spin loss mechanisms [65]. Ge/Si heterostructures, despite the presence of crystal defects that can limit the overall quantum efficiency of the radiative emission, already play a central role in microelectronic and photonic technologies and are now increasingly applied also in the quantum information realm [55,66–68]. Optical spin pumping could thus facilitate the realization of sought-after Si-based spintronic devices because it does not require the use of ferromagnetic layers. Moreover, it allows for the development of advanced integrated platforms combining photonics, spintronics, and electronics, such as spin-photon interfaces or spin-orbitronic devices.

ACKNOWLEDGMENTS

The authors would like to acknowledge A. Sammak for the epitaxy of Ge on Si, and E. Vitiello, I. D. Losciale, and M. Crippa for technical assistance with the measurements. Financial support was provided by the Air Force Office of Scientific Research under Award No. FA8655-22-1-7050 and by the European Union's Horizon Europe Research and Innovation Programme under Agreement No. 101070700. Support by the European Union (EU) under the Italian National Recovery and Resilience Plan (NRRP) of Next Generation EU partnership PE0000023-NQSTI is also acknowledged. M.V. and D.M. acknowledge support from Ministero dell'Università e della Ricerca (MUR), call PRIN 2022, project "Integrable Thz Si-based quantum cascade operation" CUP I53D23006680001.

DATA AVAILABILITY

There are no publicly available research data or software supporting this manuscript. Requests for further information or data should be sent to the authors.

[1] G. Lampel, Nuclear dynamic polarization by optical electronic saturation and optical pumping in semiconductors, Phys. Rev. Lett. **20**, 491 (1968).

[2] M. I. Dyakonov and V. I. Perel, *Optical Orientation* (Elsevier, North-Holland, New York, 1984), Chap. 2.

[3] I. Žutić, J. Fabian, and S. Das Sarma, Spintronics: Fundamentals and applications, Rev. Mod. Phys. **76**, 323 (2004).

[4] R. R. Parsons, Band-to-band optical pumping in solids and polarized photoluminescence, Phys. Rev. Lett. **23**, 1152 (1969).

[5] T. Cao, G. Wang, W. Han, H. Ye, C. Zhu, J. Shi, Q. Niu, P. Tan, E. Wang, B. Liu, and J. Feng, Valley-selective circular dichroism of monolayer molybdenum disulphide, Nat. Commun. **3**, 887 (2012).

[6] G. Sallen, L. Bouet, X. Marie, G. Wang, C. R. Zhu, W. P. Han, Y. Lu, P. H. Tan, T. Amand, B. L. Liu, and B. Urbaszek, Robust optical emission polarization in MoS_2 monolayers through selective valley excitation, Phys. Rev. B **86**, 081301(R) (2012).

[7] P. Odenthal, W. Talmadge, N. Gundlach, R. Wang, C. Zhang, D. Sun, Z.-G. Yu, Z. Valy Vardeny, and Y. S. Li, Spin-polarized exciton quantum beating in hybrid organic-inorganic perovskites, Nat. Phys. **13**, 894 (2017).

[8] H. Lu, Z. V. Vardeny, and M. C. Beard, Control of light, spin and charge with chiral metal halide semiconductors, Nat. Rev. Chem. **6**, 470 (2022).

[9] I. Žutić, J. Fabian, and S. C. Erwin, Spin injection and detection in silicon, Phys. Rev. Lett. **97**, 026602 (2006).

[10] F. Nastos, J. Rioux, M. Strimas-Mackey, B. S. Mendoza, and J. E. Sipe, Full band structure LDA and $\mathbf{k}\cdot\mathbf{p}$ calculations of optical spin-injection, Phys. Rev. B **76**, 205113 (2007).

[11] M. Cardona and F. H. Pollak, Energy-band structure of germanium and silicon: The $\mathbf{k}\cdot\mathbf{p}$ method, Phys. Rev. **142**, 530 (1966).

[12] B. T. Jonker, G. Kioseoglou, A. T. Hanbicki, C. H. Li, and P. E. Thompson, Electrical spin-injection into silicon from a ferromagnetic metal/tunnel barrier contact, Nat. Phys. **3**, 542 (2007).

[13] N. Sircar and D. Bougeard, Experimental investigation of the optical spin-selection rules in bulk Si and Ge/Si quantum dots, Phys. Rev. B **89**, 041301(R) (2014).

[14] F. Bottegoni, C. Zucchetti, F. Ciccacci, M. Finazzi, and G. Isella, Optical generation of pure spin currents at the indirect gap of bulk Si, Appl. Phys. Lett. **110**, 042403 (2017).

[15] C. Zucchetti, F. Scali, P. Grassi, M. Bollani, L. Anzi, G. Isella, M. Finazzi, F. Ciccacci, and F. Bottegoni, Non-local architecture for spin current manipulation in silicon platforms, APL Mater. **11**, 021102 (2023).

[16] L. Grenet, M. Jamet, P. Noé, V. Calvo, J.-M. Hartmann, L. E. Nistor, B. Rodmacq, S. Auffret, P. Warin, and Y. Samson, Spin injection in silicon at zero magnetic field, Appl. Phys. Lett. **94**, 032502 (2009).

[17] S. P. Dash, S. Sharma, R. S. Patel, M. P. de Jong, and R. Jansen, Electrical creation of spin polarization in silicon at room temperature, Nature (London) **462**, 491 (2009).

[18] A. Spiesser, H. Saito, Y. Fujita, S. Yamada, K. Hamaya, S. Yuasa, and R. Jansen, Giant spin accumulation in silicon nonlocal spin-transport devices, Phys. Rev. Appl. **8**, 064023 (2017).

[19] J.-C. Le Breton, S. Sharma, H. Saito, S. Yuasa, and R. Jansen, Thermal spin current from a ferromagnet to silicon by Seebeck spin tunnelling, Nature (London) **475**, 82 (2011).

[20] X. Marie, D. Lagarde, A. Balocchi, C. Robert, L. Lombez, P. Renucci, T. Amand, and F. Cadiz, Using light to polarize and detect electron spins in silicon, Phys. Rev. Lett. **134**, 106902 (2025).

[21] P. Li and H. Dery, Theory of spin-dependent phonon-assisted optical transitions in silicon, Phys. Rev. Lett. **105**, 037204 (2010).

[22] P. Li, D. Trivedi, and H. Dery, Spin-dependent optical properties in strained silicon and germanium, Phys. Rev. B **87**, 115203 (2013).

[23] K. Ando and E. Saitoh, Observation of the inverse spin Hall effect in silicon, Nat. Commun. **3**, 629 (2012).

[24] E. Shikoh, K. Ando, K. Kubo, E. Saitoh, T. Shinjo, and M. Shiraishi, Spin-pump-induced spin transport in *p*-type Si at room temperature, Phys. Rev. Lett. **110**, 127201 (2013).

[25] Y. Tserkovnyak, A. Brataas, G. E. W. Bauer, and B. I. Halperin, Nonlocal magnetization dynamics in ferromagnetic heterostructures, Rev. Mod. Phys. **77**, 1375 (2005).

[26] E. J. Loren, B. A. Ruzicka, L. K. Werake, H. Zhao, H. M. van Driel, and A. L. Smirl, Optical injection and detection of ballistic pure spin currents in Ge, Appl. Phys. Lett. **95**, 092107 (2009).

[27] J. Rioux and J. E. Sipe, Optical injection and control in germanium: Thirty-band $\mathbf{k}\cdot\mathbf{p}$ theory, Phys. Rev. B **81**, 155215 (2010).

[28] F. Pezzoli, L. Qing, A. Giorgioni, G. Isella, E. Grilli, M. Guzzi, and H. Dery, Spin and energy relaxation in germanium studied by spin-polarized direct-gap photoluminescence, Phys. Rev. B **88**, 045204 (2013).

[29] Y.-H. Kuo, Y. K. Lee, Y. Ge, S. Ren, J. E. Roth, T. I. Kamins, D. A. B. Miller, and J. S. Harris, Strong quantum-confined Stark effect in germanium quantum-well structures on silicon, Nature (London) **437**, 1334 (2005).

[30] M. Virgilio and G. Grosso, Type-I alignment and direct fundamental gap in SiGe based heterostructures, J. Phys.: Condens. Matter **18**, 1021 (2006).

[31] H. Dery, Y. Song, P. Li, and I. Žutić, Silicon spin communication, Appl. Phys. Lett. **99**, 082502 (2011).

[32] R. Jansen, Silicon spintronics, Nat. Mater. **11**, 400 (2012).

[33] I. M. Huygens, W. Gomes, and K. Strubbe, Etching of germanium in hydrogenperoxide solutions, ECS Transactions **6**, 375 (2007).

[34] D. Scharfetter and H. Gummel, Large-signal analysis of a silicon Read diode oscillator, IEEE Trans. Electron Devices **16**, 64 (1969).

[35] M. Lundstrom and R. Schuelke, Numerical analysis of heterostructure semiconductor devices, IEEE Trans. Electron Devices **30**, 1151 (1983).

[36] See Supplemental Material at http://link.aps.org/supplemental/10.1103/cdkm-m3qc for additional experimental details, sample characterization, theoretical derivations, and supporting data.

[37] F. Pezzoli, F. Bottegoni, D. Trivedi, F. Ciccacci, A. Giorgioni, P. Li, S. Cecchi, E. Grilli, Y. Song, M. Guzzi, H. Dery, and G. Isella, Optical spin injection and spin lifetime in Ge heterostructures, Phys. Rev. Lett. **108**, 156603 (2012).

[38] S. De Cesari, R. Bergamaschini, E. Vitiello, A. Giorgioni, and F. Pezzoli, Optically reconfigurable polarized emission in germanium, Sci. Rep. **8**, 11119 (2018).

[39] C. Wang, J. Chen, R. Becker, and A. Zdetsis, Second order Raman spectrum and phonon density of states of silicon, Phys. Lett. A **44**, 517 (1973).

[40] P. A. Temple and C. E. Hathaway, Multiphonon Raman spectrum of silicon, Phys. Rev. B **7**, 3685 (1973).

[41] P. J. Dean, J. R. Haynes, and W. F. Flood, New radiative recombination processes involving neutral donors and acceptors in silicon and germanium, Phys. Rev. **161**, 711 (1967).

[42] P. M. Colley and E. C. Lightowlers, Calibration of the photoluminescence technique for measuring B, P and Al concentrations in Si in the range 10^{12} to 10^{15} cm^{-3} using Fourier transform spectroscopy, Semicond. Sci. Technol. **2**, 157 (1987).

[43] G. Davies, The optical properties of luminescence centres in silicon, Phys. Rep. **176**, 83 (1989).

[44] F. Pezzoli, E. Bonera, E. Grilli, M. Guzzi, S. Sanguinetti, D. Chrastina, G. Isella, H. von KÃ¤nel, E. Wintersberger, J. Stangl, and G. Bauer, Raman spectroscopy determination of composition and strain in $Si_{1-x}Ge_x$/Si heterostructures, Mater. Sci. Semicond. Process. **11**, 279 (2008).

[45] F. Pezzoli, E. Bonera, E. Grilli, M. Guzzi, S. Sanguinetti, D. Chrastina, G. Isella, H. von Kaenel, E. Wintersberger, J. Stangl, and G. Bauer, Phonon strain shift coefficients in $Si_{1-x}Ge_x$ alloys, J. Appl. Phys. **103**, 093521 (2008).

[46] A. Sammak, D. Sabbagh, N. W. Hendrickx, M. Lodari, B. Paquelet Wuetz, A. Tosato, L. Yeoh, M. Bollani, M. Virgilio, M. A. Schubert, P. Zaumseil, G. Capellini, M. Veldhorst, and G. Scappucci, Shallow and undoped germanium quantum wells: A playground for spin and hybrid quantum technology, Adv. Funct. Mater. **29**, 1807613 (2019).

[47] E. Vitiello, M. Virgilio, A. Giorgioni, J. Frigerio, E. Gatti, S. De Cesari, E. Bonera, E. Grilli, G. Isella, and F. Pezzoli, Spin-dependent direct gap emission in tensile-strained Ge films on Si substrates, Phys. Rev. B **92**, 201203(R) (2015).

[48] C. G. Van de Walle and R. M. Martin, Theoretical calculations of heterojunction discontinuities in the Si/Ge system, Phys. Rev. B **34**, 5621 (1986).

[49] C. G. Van de Walle, Band lineups and deformation potentials in the model-solid theory, Phys. Rev. B **39**, 1871 (1989).

[50] R. Geiger, J. Frigerio, M. J. Süess, D. Chrastina, G. Isella, R. Spolenak, J. Faist, and H. Sigg, Excess carrier lifetimes in Ge layers on Si, Appl. Phys. Lett. **104**, 062106 (2014).

[51] F. Pezzoli, F. Isa, G. Isella, C. V. Falub, T. Kreiliger, M. Salvalaglio, R. Bergamaschini, E. Grilli, M. Guzzi, H. von Känel, and L. Miglio, Ge crystals on Si show their light, Phys. Rev. Appl. **1**, 044005 (2014).

[52] F. Pezzoli, A. Giorgioni, K. Gallacher, F. Isa, P. Biagioni, R. W. Millar, E. Gatti, E. Grilli, E. Bonera, G. Isella, D. J. Paul, and L. Miglio, Disentangling nonradiative recombination processes in Ge micro-crystals on Si substrates, Appl. Phys. Lett. **108**, 262103 (2016).

[53] W. Shockley and W. T. Read, Statistics of the recombinations of holes and electrons, Phys. Rev. **87**, 835 (1952).

[54] A. Giorgioni, E. Vitiello, E. Grilli, M. Guzzi, and F. Pezzoli, Valley-dependent spin polarization and long-lived electron spins in germanium, Appl. Phys. Lett. **105**, 152404 (2014).

[55] A. Giorgioni, S. Paleari, S. Cecchi, E. Vitiello, E. Grilli, G. Isella, W. Jantsch, M. Fanciulli, and F. Pezzoli, Strong confinement-induced engineering of the *g* factor and lifetime of conduction electron spins in Ge quantum wells, Nat. Commun. **7**, 13886 (2016).

[56] D. H. Goldstein, *Polarized Light* (Taylor & Francis, London, 2010).

[57] N. A. Drozdow, A. A. Patrin, and V. D. Tkachev, Recombination radiation on dislocations in silicon, Pis'ma Zh. Eksp. Teor. Fiz. **23**, 11 (1976) [JETP Lett. **23**, 597 (1978)].

[58] M. Reiche and M. Kittler, Electronic and optical properties of dislocations in silicon, Crystals **6**, 74 (2016).

[59] E. Vitiello, S. Rossi, C. A. Broderick, G. Gravina, A. Balocchi, X. Marie, E. P. O'Reilly, M. Myronov, and F. Pezzoli, Continuous-wave magneto-optical determination of the carrier lifetime in coherent $Ge_{1-x}Sn_x$/Ge heterostructures, Phys. Rev. Appl. **14**, 064068 (2020).

[60] R. L. Watters and G. W. Ludwig, Measurement of minority carrier lifetime in silicon, J. Appl. Phys. **27**, 489 (1956).

[61] D. Schroder, Carrier lifetimes in silicon, IEEE Trans. Electron Devices **44**, 160 (1997).

[62] J. Schmidt and A. G. Aberle, Accurate method for the determination of bulk minority-carrier lifetimes of mono- and multicrystalline silicon wafers, J. Appl. Phys. **81**, 6186 (1997).

[63] G. Grzybowski, R. Roucka, J. Mathews, L. Jiang, R. T. Beeler, J. Kouvetakis, and J. Menéndez, Direct versus indirect optical recombination in Ge films grown on Si substrates, Phys. Rev. B **84**, 205307 (2011).

[64] H. Lee, S.-H. Choi, and T.-Y. Seong, Origin of dislocation-related photoluminescence bands in very thin silicon-germanium layers grown on silicon substrates, Appl. Phys. Lett. **71**, 3823 (1997).

[65] J.-M. Tang, B. T. Collins, and M. E. Flatté, Electron spin-phonon interaction symmetries and tunable spin relaxation in silicon and germanium, Phys. Rev. B **85**, 045202 (2012).

[66] R. Pillarisetty, Academic and industry research progress in germanium nanodevices, Nature (London) **479**, 324 (2011).

[67] N. Na, Y.-C. Lu, Y.-H. Liu, P.-W. Chen, Y.-C. Lai, Y.-R. Lin, C.-C. Lin, T. Shia, C.-H. Cheng, and S.-L. Chen, Room temperature operation of germanium-silicon single-photon avalanche diode, Nature (London) **627**, 295 (2024).

[68] G. Scappucci, C. Kloeffel, F. A. Zwanenburg, D. Loss, M. Myronov, J.-J. Zhang, S. De Franceschi, G. Katsaros, and M. Veldhorst, The germanium quantum information route, Nat. Rev. Mater. **6**, 926 (2020).